

## Supporting Information

### **Self-Tandem Catalysis of Fast Mg<sup>2+</sup> Desolvation and Sulfur Conversions for Ultrahigh-Performance Mg-S Battery via Serially-Assembled Atomic Reactors**

Qinghua Guan<sup>1,3,†</sup>, Jian Wang<sup>1,2,9,†,\*</sup>, Quan Zhuang<sup>†,5</sup>, Jing Zhang<sup>6</sup>, Linge Li<sup>1,3</sup>, Lujie Jia<sup>1</sup>, Yongzheng Zhang<sup>7</sup>, Hongfei Hu<sup>1,3</sup>, Huimin Hu<sup>1</sup>, Shuang Cheng<sup>1,3</sup>, Huang Zhang<sup>8</sup>, Huihua Li<sup>8</sup>, Meinan Liu<sup>1,3</sup>, Shuangyin Wang<sup>4,\*</sup> & Hongzhen Lin<sup>1,3,\*</sup>

<sup>1</sup> *i*-Lab & CAS Key Laboratory of Nanophotonic Materials and Devices, Suzhou Institute of Nano-Tech and Nano-Bionics, Chinese Academy of Sciences, Suzhou 215123, China

<sup>2</sup> Helmholtz Institute Ulm (HIU), Ulm D89081, Germany

<sup>3</sup> School of Nano-Tech and Nano-Bionics, University of Science and Technology of China, Hefei 230026, China

<sup>4</sup> State Key Laboratory of Chemo/Bio-Sensing and Chemometrics, College of Chemistry and Chemical Engineering, Hunan University, Changsha 410082, China

<sup>5</sup> Inner Mongolia Key Laboratory of Carbon Nanomaterials, Nano Innovation Institute (NII), College of Chemistry and Materials Science, Inner Mongolia Minzu University, Tongliao 028000, China

<sup>6</sup> School of Materials Science and Engineering, Xi'an University of Technology, Xi'an 710048, China

<sup>7</sup> State Key Laboratory of Chemical Engineering, East China University of Science and Technology, Shanghai 200237, China

<sup>8</sup> Key Laboratory of Engineering Dielectric and Applications (Ministry of Education), School of Electrical and Electronic Engineering, Harbin University of Science and Technology, Harbin 150080, China

<sup>9</sup> Karlsruhe Institute of Technology (KIT), Karlsruhe D-76021, Germany

† These authors contributed to this work equally.

Corresponding authors: wangjian2014@sinano.ac.cn; jian.wang@kit.edu

shuangyinwang@hnu.edu.cn

hzlin2010@sinano.ac.cn

## **Experimental section**

### **Synthesis and fabrication of the STAR@LCNC**

The ZIF-8/CNT precursor was synthesized by an improved method. The CNT powders (45 mg) and polyvinyl pyrrolidone (PVP) (300 mg) were sonicated in methanol (60 mL) for 40 min, followed by gradually adding 2-MeIm (0.7539 g) to the as-prepared CNT solution with stirring for 0.5 h, then 60 mL of a methanol solution with  $\text{Zn}(\text{NO}_3)_2 \cdot 6\text{H}_2\text{O}$  (1.3521 g) was added to the above dispersion. The mixed dispersion was stirring for 5 min before leaving undisturbed at room temperature for 24 h. After filtration, washing, and freezing-drying for 12 h, the ZIF-8/CNT composites was collected and carbonized in a sealed vessel under flowing  $\text{NH}_3/\text{Ar}$  (5%: 95%, by volume) atmosphere at 500 °C with a heating rate of 5 °C  $\text{min}^{-1}$  and kept for 120 min at 500 °C. Finally, the STAR@LCNC composites were achieved after cooling down to room temperature naturally.

### **Synthesis of STAR@LCNC-S and CNT-S composites**

The as-synthesized STAR@LCNC composites were mixed with commercial sulfur by thoroughly grinding with the mass ratio of 1: 3. The obtained mixtures were heated in a sealed vessel under flowing argon atmosphere at 155 °C for 12 h. After cooling down to room temperature, the STAR@LCNC-S composites were obtained. Similarly, the CNT-S was made by the same method. The CNT powders were mixed with commercial sulfur by thoroughly grinding with the mass ratio of 1: 3. The obtained mixtures were heated in a sealed vessel under flowing argon atmosphere at 155 °C for 12 h. After cooling down to room temperature, the CNT-S composites were obtained.

### **Synthesis of the magnesium polysulfides (MgPSs) solution**

The roughly-estimated 0.23 mol  $\text{L}^{-1}$  MgPSs solution (the denoted concentration is based on atomic magnesium in the reaction mixture) was prepared by mixing 27.83 mg of Mg powder, 300 mg of sulfur powder, 42.39 mg of LiCl, 47.5 mg of  $\text{MgCl}_2$  and 5 ml solvent of electrolyte (THF) together and then stirred continuously for 24 h at room

temperature. The optical visual chemical interactions were studied via immersing the equal amount (10 mg) of CNT or STAR@LCNC into magnesium polysulfide solution.

### **Fabrication of magnesium-sulfur coin cells**

To prepare the cathodes, STAR@LCNC-S composite was mixed with conductive carbon black and polyvinylidene fluoride (PVDF) binder (70: 20: 10 by weight) in N-methyl-2-pyrrolidone (NMP) solution under vigorous stirring for several times. The slurry was then spread onto a carbon-coated copper foil and then dried in a vacuum oven at 50 °C for 48 h to fully evaporate the NMP. Cathode chips of 10 mm in diameter were punched out with an average sulfur loading of  $\sim 1.0 \text{ mg cm}^{-2}$ . The 2025-type coin cells were prepared in a glove box filled with highly pure Ar gas, using magnesium foils as the anodes (the thickness of the magnesium foil anode is 0.1 mm and the diameter of the magnesium foil anode is 15 mm), and  $\text{MgCl}_2\text{-LiCl/THF}$  ( $0.4 \text{ mol L}^{-1} \text{ MgCl}_2$ ,  $0.8 \text{ mol L}^{-1} \text{ LiCl}$  in tetrahydrofuran) as the electrolyte, and Whatman Glass fiber as the separator. Before assembling, 120  $\mu\text{L}$  electrolyte was added into the cell, then assembled quickly to prevent volatilization of electrolyte.

### **Polysulfide conversion and MgS precipitation**

To prepare the electrode without any sulfur, the bare STAR@LCNC or CNT composite was mixed with conductive carbon black and PVDF binder (70: 20: 10 by weight) in NMP solution under vigorous stirring for several times, respectively. Then the slurry was coated onto a carbon film and then dried in a vacuum oven at 50 °C for 48 h to fully evaporate the NMP. Cathode chips of 10 mm in diameter were punched out with an average loading of  $\sim 0.65 \text{ mg cm}^{-2}$ . The 2025-type coin cells were prepared in a glove box filled with highly pure Ar gas,  $\text{MgCl}_2\text{-LiCl/THF}$  as the electrolyte, and Whatman Glass fiber as the separator. For symmetric cells, the electrodes of STAR@LCNC or CNT composite acts as both working electrode and the counter electrode, respectively. For the asymmetric cells, the counter electrode is Mg anode. 70

$\mu\text{L}$  normal electrolyte and 30  $\mu\text{L}$  above magnesium polysulfide solution was added into the cell or one the electrode surface before assembling.

### **Magnesium-ion migration number test**

The magnesium-magnesium symmetrical battery consists of two same magnesium foils with different coatings (CNT or STAR@LCNC) as cathode and anode. The bare STAR@LCNC or CNT composite was mixed with conductive carbon black and PVDF binder (70: 20: 10 by weight) in NMP solution under vigorous stirring for several times, respectively. Then the slurry was coated onto magnesium foils and then dried in a vacuum oven at 50 °C for 48 h to fully evaporate the NMP. The magnesium-ions migration number was measured by i-t Amperometric technique, a small and constant potential difference  $\Delta V$  (10 mV) is applied to the measured symmetrical cell while the change in current over time is recorded, and calculated by the following equation:

$$t_{Mg^{2+}} = I_s / I_0$$

where  $I_s$  and  $I_0$  represent the currents at the steady state and initial state, respectively.

### **Material characterization**

A Hitachi S4800 field-emission scanning electron microscope was utilized to observe the morphology and structure of the samples. A Themis aberration-corrected scanning transmission electron microscope (AC-STEM) was used to characterize the single zinc atoms operated at 300 kV. The presented chemical elements were analyzed by energy-dispersive X-ray spectroscopy (EDX, Quanta FEG 250) operated at 30 kV. X-ray diffraction (XRD, Bruker D8) was used to characterize the crystal structure of the composites. The thermogravimetric analysis was performed on a TG/DTA 6200 to determine the weight of sulfur on the two matrices from room temperature to 500 °C under the atmosphere of  $\text{N}_2$  with the heating rate of 10 °C  $\text{min}^{-1}$ . X-ray photoelectronic spectroscopy (XPS) data were collected in an ESCALAB 250XI (Thermo Scientific) spectrometer to measure the chemical surroundings of different elements in the composites and cathodes at different electrochemical stages. Commercial device the *in-*

*situ* sum frequency generation (SFG) picosecond laser system using a copropagating configuration is used for with/without the bias voltage of 100 mV on the electrode/solvent interface with/without STAR@LCNC or CNT layer. The visible green light wavelength is 532 nm and the IR pulse are adjustable ranging from 1000 to 4000  $\text{cm}^{-1}$ . The incident angle is  $60^\circ$  for the visible beam, and  $55^\circ$  for the IR beam. The time-of-flight secondary-ion mass spectrometry (TOF-SIMS) data were collected from TOF.SIMS 5-100 to observe the 3D distribution and depth information of each species. The electrochemical impedance spectroscopy measurements of the coin cells were completed on a VMP-3 electrochemical working station with the frequency ranging from 200 kHz to 100 mHz. Cyclic voltammetry was carried out with the coin cell configuration on the same electrochemical working station within the range of 0.2-2.0 V at  $0.05 \text{ mV s}^{-1}$ . Electrochemical cycling measurements were carried out on Land CT2001 automatic battery test systems between 0.2 and 1.7 V at designated rates.

### **Computational Details**

The desolvation free energy were estimated by Gaussian 16 software. The geometrical optimizations and energy calculations of the models were performed at the B3LYP/6-31 G(d, p) level. Vibrational frequencies were analyzed at the same level to verify the obtained structures at local energy minima. In addition, SMD polarized continuum mode with THF as the solvent was taken into consideration in all calculations, and the correction of 1.89 kcal/mol was also included to account for the standard state conversion from the gas phase to the solution. The density functional theory (DFT) calculations were performed to study the structural and electronic properties within the Vienna ab initio Simulation Package (VASP) code.<sup>S19</sup> The projected augmented wave (PAW) method was used to describe the electron-ion interaction,<sup>S20</sup> and the generalized gradient approximation (GGA) with the function of Perdew-Burke-Ernzerhof (PBE) was used to describe exchange-correlation energy.<sup>S21</sup> The cut-off energy of 500 eV was selected with a plane-wave basis set. A  $5 \times 5 \times 1$  Monkhorst-Pack is used for the k-mesh sampling in the first Brillouin zone. All the

atoms were relaxed until the energy change was less than  $10^{-4}$  eV for the electronic relaxation and the forces on each atom were less than  $0.01$  eV  $\text{\AA}^{-1}$  for the ionic relaxation. The DFT-D3 empirical correction method was employed to describe van der Waals interactions. To evaluate delithiation reaction kinetics, the barriers for  $\text{Mg}_2\text{S}_2$  decomposition on carbon and STAR@LCNC were calculated with the climbing-image nudged elastic band (CI-NEB) method. Device Studio program provides a number of functions for performing visualization, modeling and simulation. And CI-NEB simulations were performed by DS-PAW software integrated in Device Studio program.<sup>S22</sup> We used the VASPKIT code for postprocessing of the VASP calculated data.<sup>S23</sup> The models of carbon, nitrogen-doped carbon, and Zn atoms embedded nitrogen-doped carbon are labelled as carbon, NC, STAR@LCNC. The adsorption energies ( $E_{ads}$ ) are defined as:

$$E_{ads} = E_{total} - E_{surface} - E_{cluster}$$

where  $E_{surface}$ ,  $E_{cluster}$ ,  $E_{total}$  are the total energies of the clean substrate, the isolated S-containing cluster, and the substrate adsorbed with S-containing clusters, respectively.

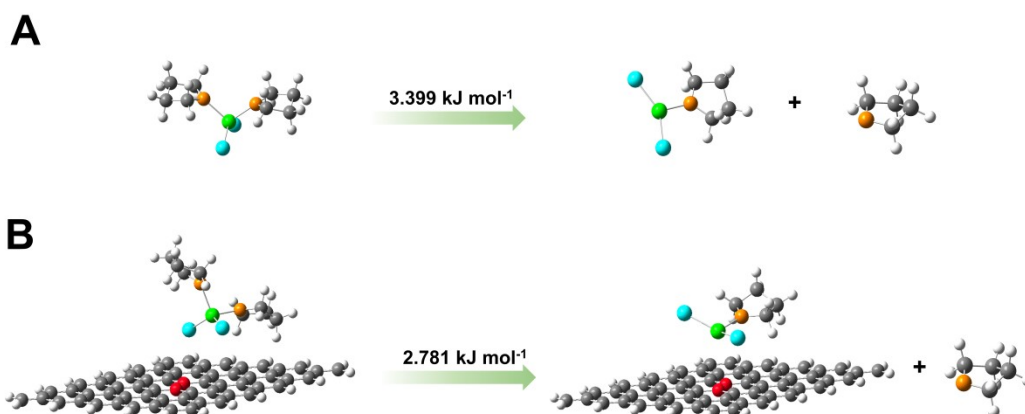


**Figure S1.** Desolvation barrier of  $\text{MgCl}_2(\text{THF})_2$  into  $\text{MgCl}_2 \cdot \text{THF}$  and THF (A) in liquid electrolyte or (B) on NC, respectively.

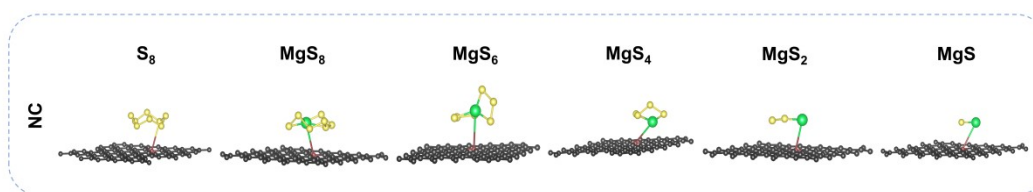


**Figure S2.** The corresponding structure illustrations of different  $\text{S}_8$ ,  $\text{MgS}_8$ ,  $\text{MgS}_6$ ,  $\text{MgS}_4$ ,  $\text{MgS}_2$  and  $\text{MgS}$  on NC substrates.

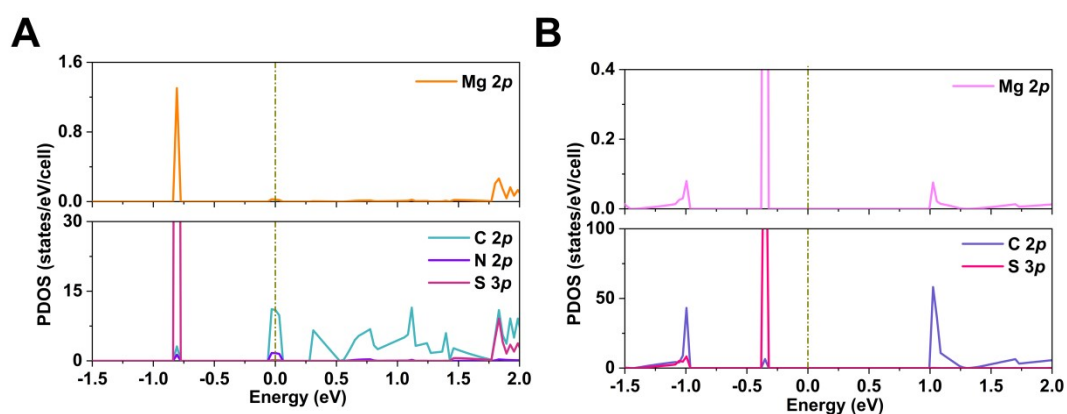


**Figure S3.** The projected density of states (PDOS) for the adsorbed configuration of  $\text{MgS}_4$  on (A) NC and (B) pristine carbon.

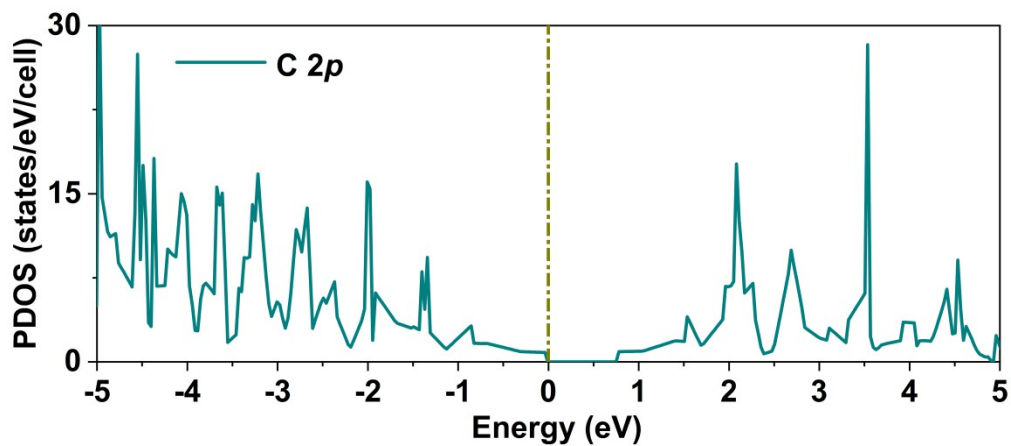


**Figure S4.** The projected density of states (PDOS) for pristine carbon.

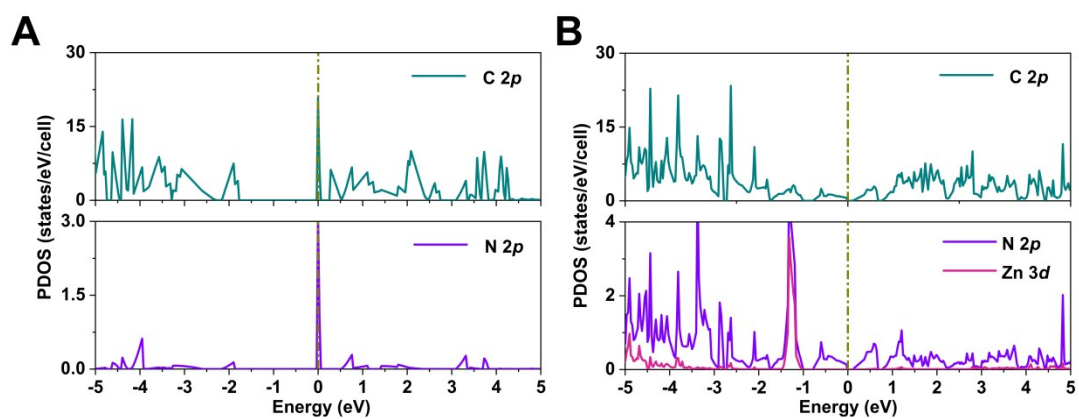


**Figure S5.** The projected density of states (PDOS) for (A) NC and (B) STAR@LCNC.

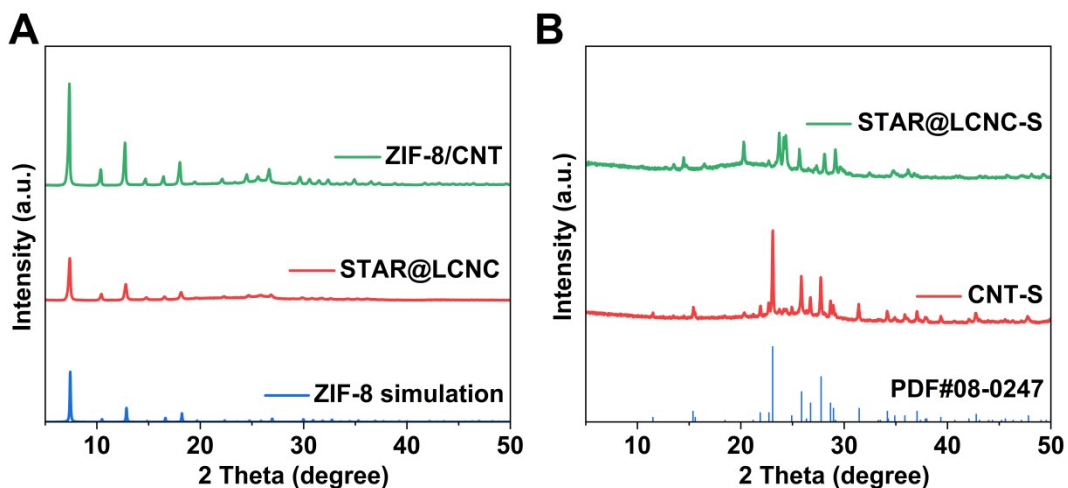


**Figure S6.** (A) XRD patterns of ZIF-8/CNT and STAR@LCNC, the simulated pattern of ZIF-8 is also listed as a reference. (B) XRD patterns of STAR@LCNC-S and CNT-S.

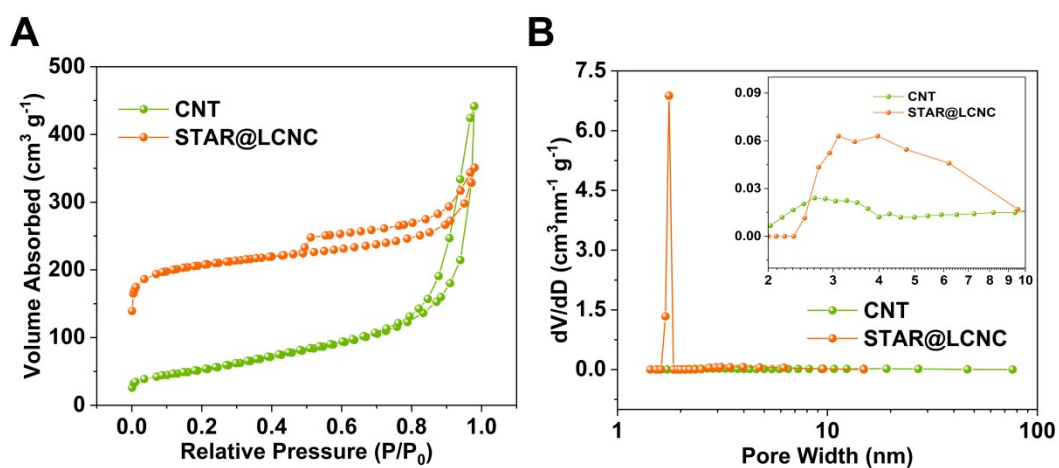


**Figure S7.** (A) N<sub>2</sub> adsorption–desorption isotherms of STAR@LCNC and CNT composites. (B) Corresponding pore size distribution of STAR@LCNC and CNT.

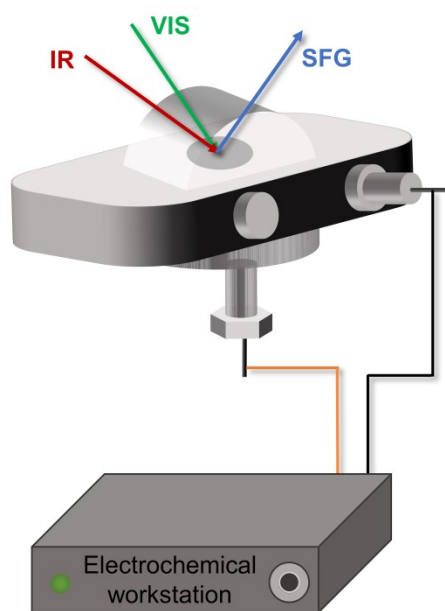


**Figure S8.** Schematic diagram of the *in-situ* SFG.

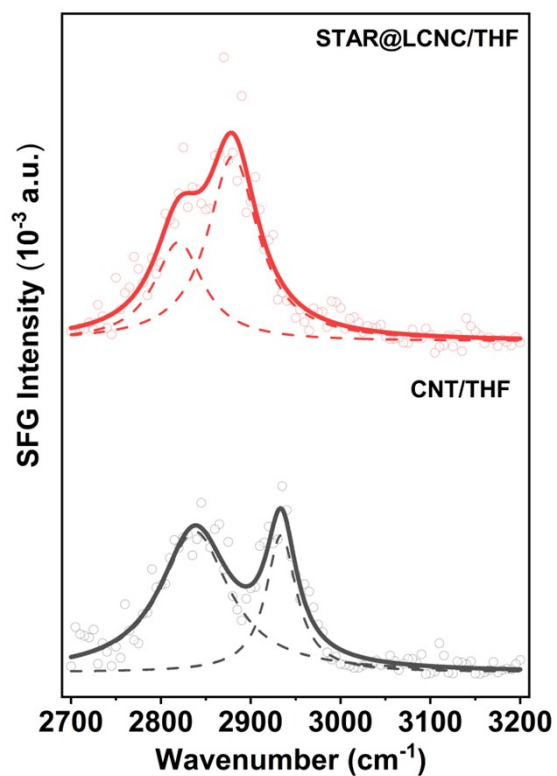


**Figure S9.** The SFG spectra of different adsorption states of  $\text{Mg}^{2+}$  solvation structure in pure THF.

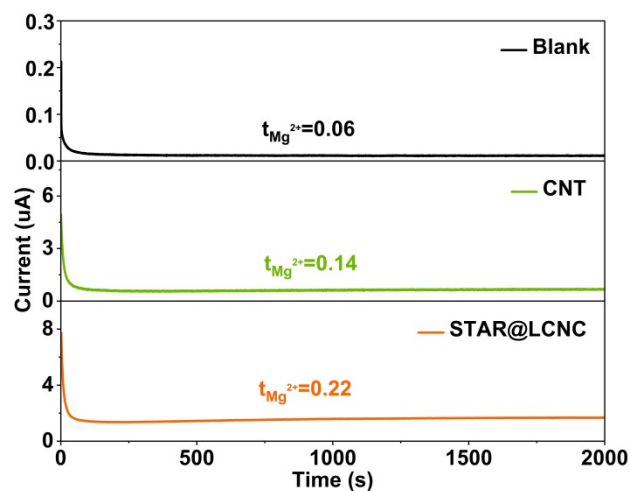


**Figure S10.** Magnesium ion migration number for blank magnesium foil, CNT and STAR@LCNC materials.

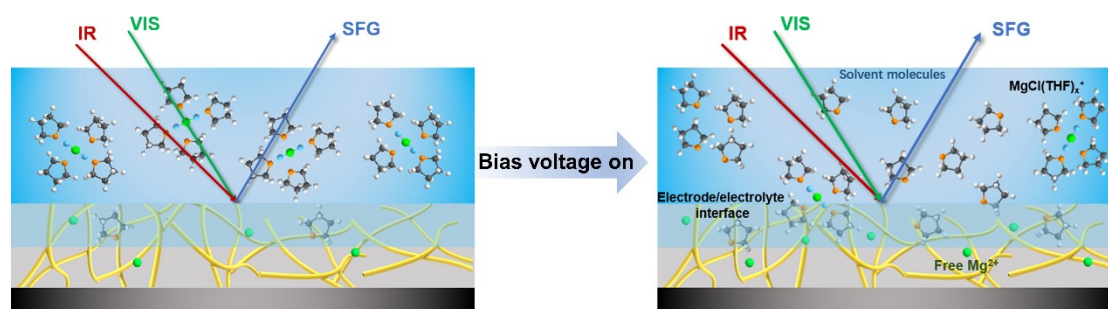


**Figure S11.** The molecular states of the  $\text{Mg}^{2+}$  solvation structure in the CNT electrode/electrolyte interface before and after turning bias voltage on.

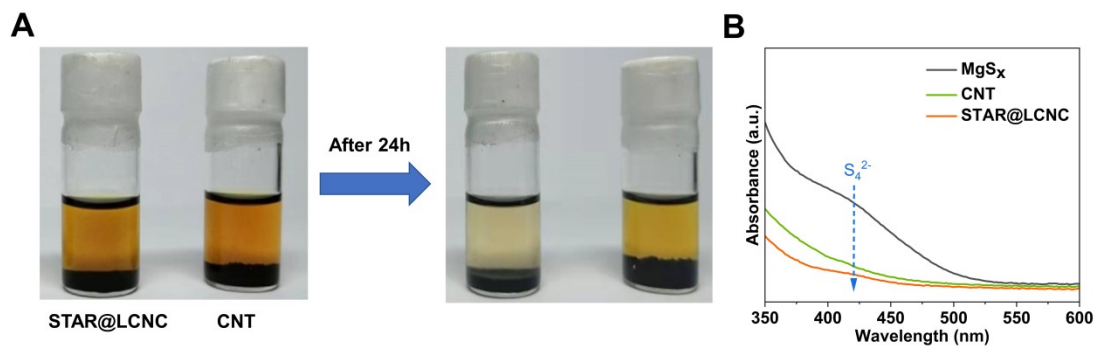


**Figure S12.** (A) Optical coloration photos of polysulfide solution with STAR@LCNC and CNT powder before and after sufficient interaction. (B) UV-vis spectra of corresponding remained  $MgS_x$  solution.

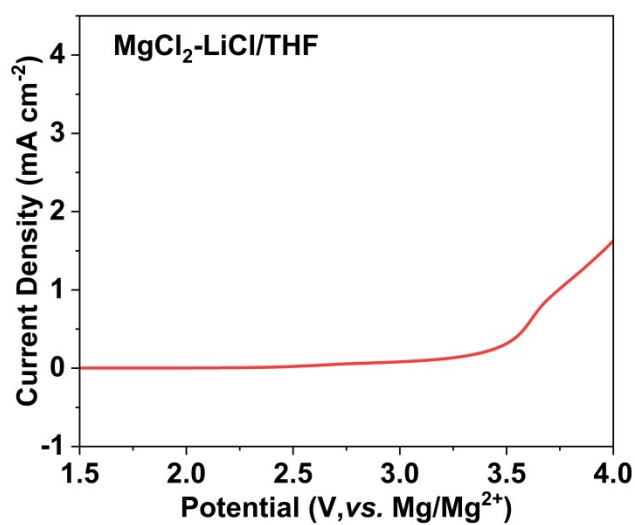


**Figure S13.** Linear sweep voltammetry (LSV) of the  $MgCl_2-LiCl/THF$  electrolyte (the working electrode is stainless steel; the counter and reference electrodes are Mg foils).

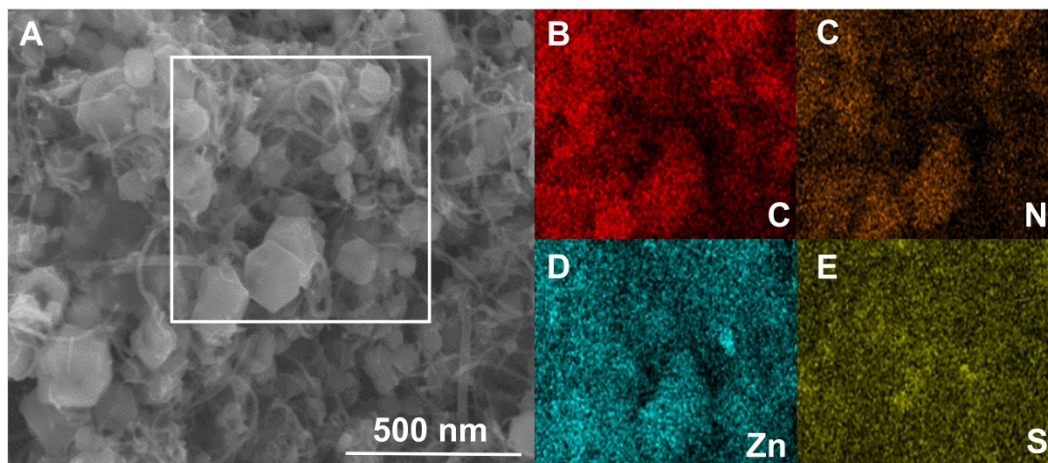


**Figure S14.** (A) SEM images of the STAR@LCNC-S electrode, and the corresponding EDS elemental mapping of (B) C, (C) N, (D) Zn and (E) S corresponding to the area in (A).

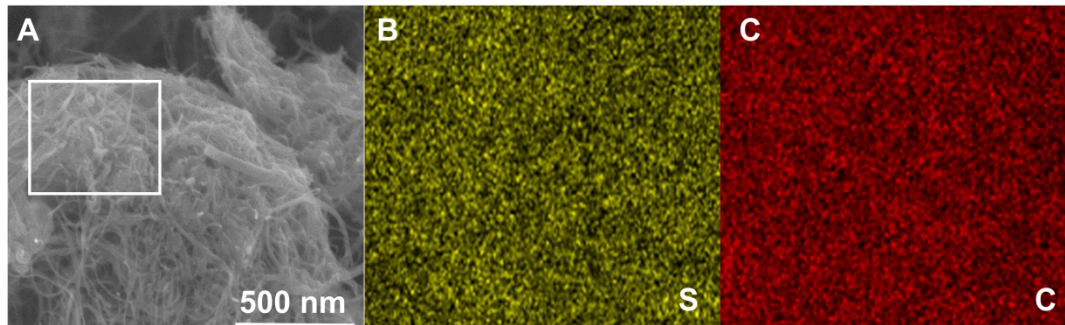


**Figure S15.** (A) SEM images of the CNT-S electrode, and the corresponding EDS elemental mapping of (B) S and (C) C corresponding to the area in (A).

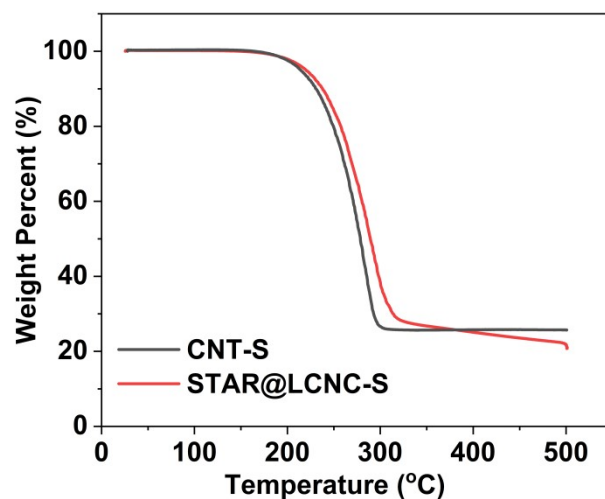


**Figure S16.** TG curves of CNT-S and STAR@LCNC-S powder in  $N_2$  atmosphere with a heating rate of  $10\text{ }^\circ\text{C min}^{-1}$ , respectively.

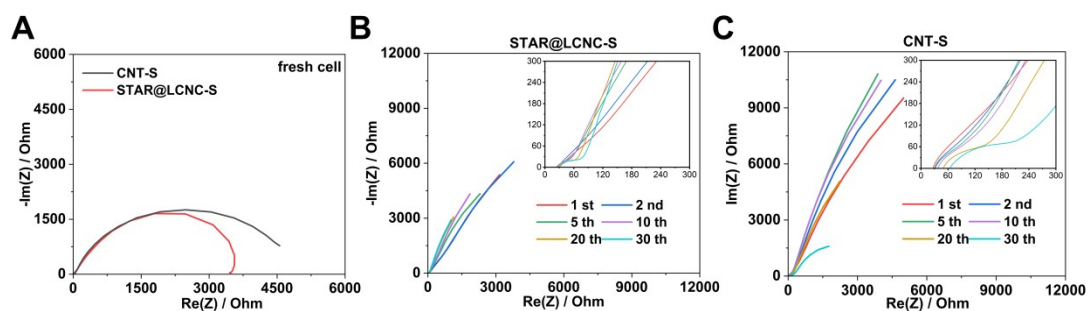


**Figure S17.** (A) The EIS comparison of the fresh cells with STAR@LCNC-S electrode and CNT-S electrode. The EIS comparison of the (B) STAR@LCNC-S electrode and (C) CNT-S electrode at different cycles.

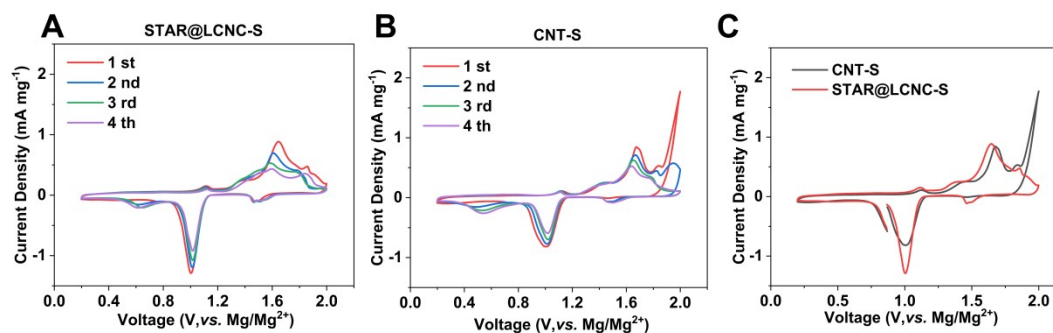


**Figure S18.** CV profiles of the (A) STAR@LCNC-S electrode and (B) CNT-S electrode cycled at 0.05 mV s<sup>-1</sup>. (C) Comparison of CV profiles of the CNT-S and STAR@LCNC-S electrodes in the first circle.

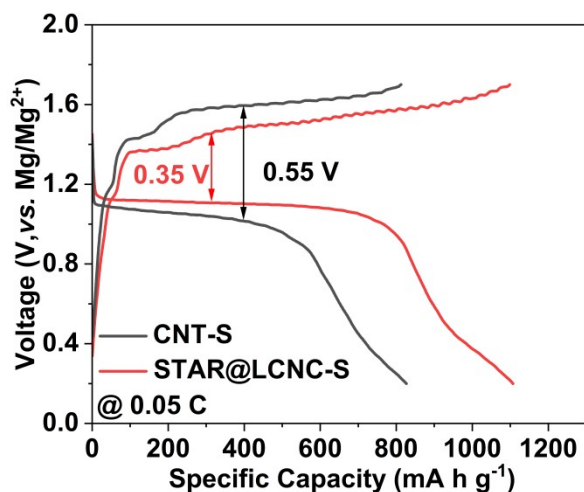


**Figure S19.** Initial galvanostatic voltage profiles of the two corresponding cells at 0.05 C.

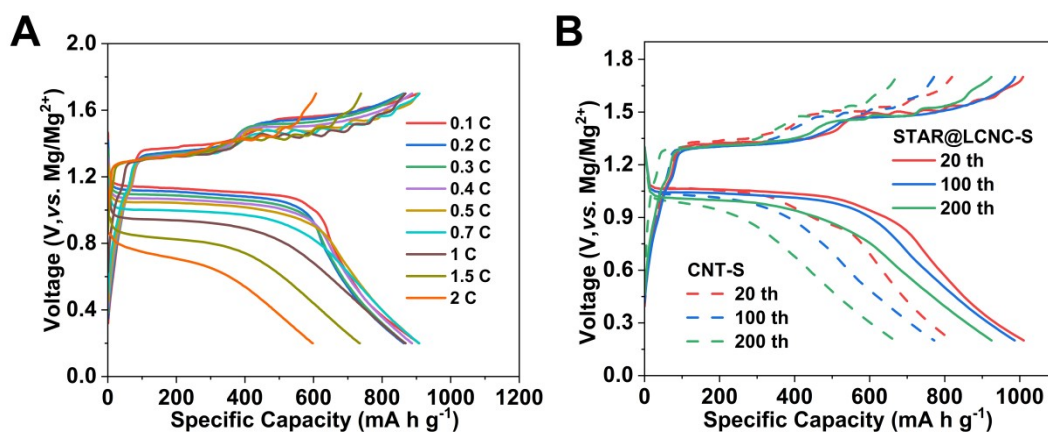


**Figure S20.** (A) Galvanostatic charge/discharge voltage profiles of STAR@LCNC-S electrode cycled at different rates. (B) The charge/discharge curve behaviors of the STAR@LCNC-S and CNT-S electrodes at 0.5 C after different cycles.

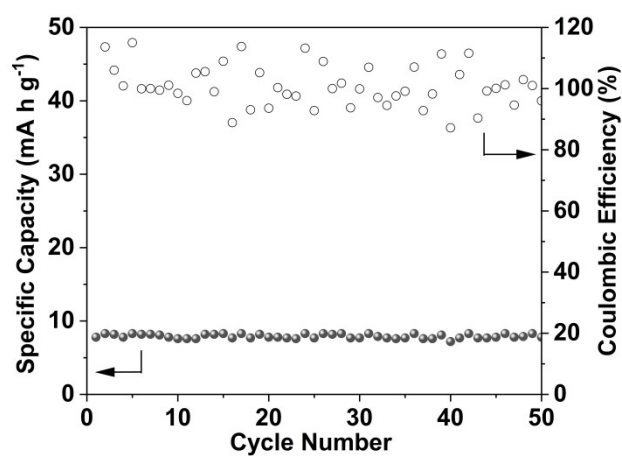


**Figure S21.** Cycling performance of the bare STAR@LCNC matrix electrodes.

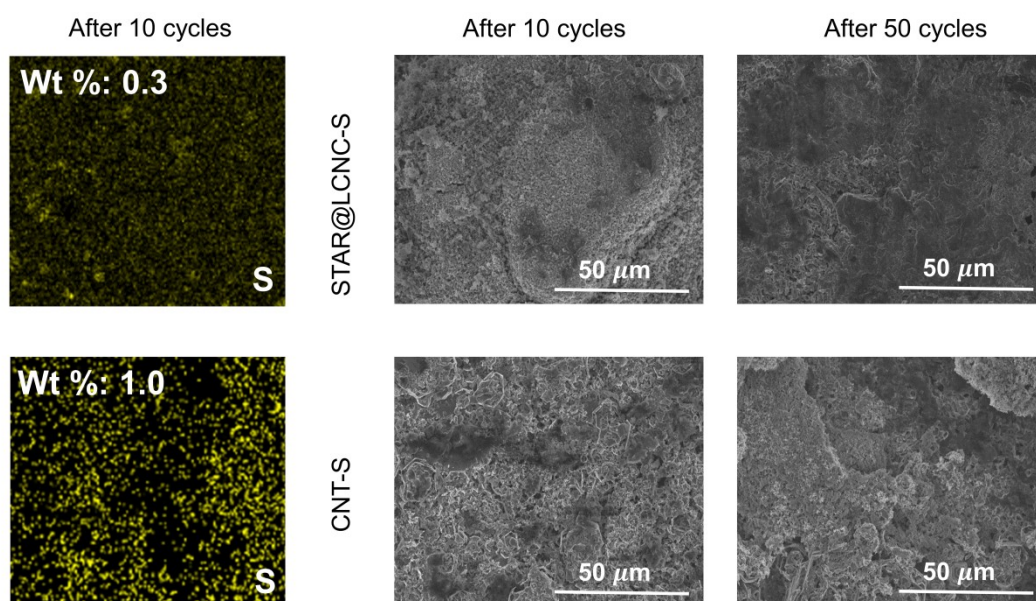


**Figure S22.** The morphologies and corresponding mapping of the corresponding Mg anodes after different cycles.

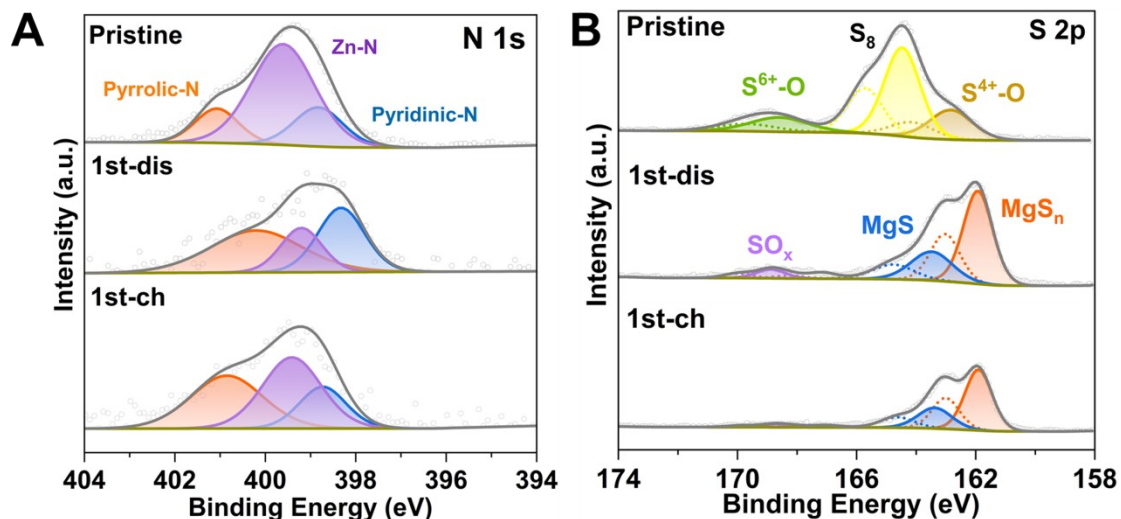


**Figure S23.** The high-resolution XPS of (A) N 1s, and (B) S 2p for pristine, fully charged, fully discharged STAR@LCNC-S electrodes.

**Table S1.** Adsorption energies  $E_{\text{ads}}$  (eV) of sulfur/magnesium polysulfides adsorption on the surfaces of carbon, NC, and STAR@LCNC.

	Carbon	NC	STAR@LCNC
$\text{S}_8$	-0.74	-0.64	-0.76
$\text{MgS}_8$	-0.86	-0.73	-1.46
$\text{MgS}_6$	-1.02	-1.25	-1.62
$\text{MgS}_4$	-0.88	-0.81	-1.67
$\text{MgS}_2$	-0.67	-0.72	-1.42
$\text{MgS}$	-0.8	-0.73	-2.66

**Table S2.** The comparison of rate performances between ours and previous reports.

Electrode material	Voltage window/V	Rate/C					Reference
		Capacity/mA h g <sup>-1</sup>					
S@pPAN	0.5-1.7	0.05	0.1	0.2	0.3	0.5	S1
		1080	700	460	210	100	
S@CNT	0.5-2.8	0.05	0.1	0.2	0.5		S2
		642	302	208	98		
KB/S	0.5-2.5	0.05	0.1	0.2	0.5	1	S3
		650	420	220	100	50	
Co <sub>3</sub> S <sub>4</sub> @MXene-S	0.4-2.1	0.1	0.2	0.5	1	2	S4
		1144	739	632	410	297	
S <sub>0.96</sub> Se <sub>0.04</sub> @CMK3	0.2-1.7	0.05	0.1	0.2	0.5	1	S5
		680	470	311	247	186	
<b>STAR@LCNC-S</b>	<b>0.2-1.7</b>	<b>0.1</b>	<b>0.5</b>	<b>1</b>	<b>1.5</b>	<b>2</b>	<b>This work</b>
		<b>925</b>	<b>900</b>	<b>860</b>	<b>740</b>	<b>610</b>	

**Table S3.** Comparison of electrochemical performance of magnesium-sulfur batteries with previous reports.

<b>Cathode</b>	<b>S Loading (wt%)</b>	<b>Electrolyte</b>	<b>Long cycling rate/C</b>	<b>Initial capacity /mA h g<sup>-1</sup></b>	<b>Cycle number</b>	<b>Capacity retention /mA h g<sup>-1</sup></b>	<b>Reference</b>
<b>S@pPAN</b>	47.3	0.2 mol L <sup>-1</sup> MBA-(MgCl <sub>2</sub> ) <sub>2</sub> -(AlCl <sub>3</sub> ) <sub>2</sub> + 1.0 mol L <sup>-1</sup> LiCl/ THF	0.1	800	85	514.8	S1
<b>S@CNT</b>	88	Mg(HMDS) <sub>2</sub> /AlCl <sub>3</sub> (1:2 ratio) in DOL/DME	0.05	654	100	270	S2
<b>KB/S</b>	50	Mg[B(hfip) <sub>4</sub> ] <sub>2</sub> /DME electrolyte (0.3 mol L <sup>-1</sup> )	0.1	460	100	310	S3
<b>Co<sub>3</sub>S<sub>4</sub>@MXene-S</b>	75	0.4 mol L <sup>-1</sup> (MgPhCl)-AlCl <sub>3</sub> in the solution of THF	0.1	1220	100	527	S4
<b>S<sub>0.96</sub>Se<sub>0.04</sub>@CMK3</b>	80	0.4 mol L <sup>-1</sup> (PhMgCl) <sub>2</sub> -AlCl <sub>3</sub> + 1 mol L <sup>-1</sup> LiCl/THF	0.1	1193.2	110	492.9	S5
<b>S/CMK-3</b>	55	MgBOR(hfip)/DEG-TEG	0.1	400	100	200	S6
<b>S@ACC</b>	/	0.4 mol L <sup>-1</sup> MgBhfip /DME	0.1	1000	60	320	S7

<b>ZIF-C-S</b>	47	0.5 mol L <sup>-1</sup> Mg(HMDS) <sub>2</sub> +1 mol L <sup>-1</sup> AlCl <sub>3</sub> +1 mol L <sup>-1</sup> LiTFSI in digylme	0.1	794.5	250	457.2	S8
<b>S@ACC</b>	/	1.0 mol L <sup>-1</sup> MgTFSI <sub>2</sub> /MgCl <sub>2</sub> /DME	0.06	869	110	600	S9
<b>S@MC</b>	55.8	0.6 mol L <sup>-1</sup> MBA–2MgCl <sub>2</sub> + 0.4 mol L <sup>-1</sup> AlCl <sub>3</sub> + 1.0 mol L <sup>-1</sup> LiCl/THF	0.1	1116.1	80	518.3	S10
<b>S@MC</b>	55	0.25 mol L <sup>-1</sup> Mg(CF <sub>3</sub> SO <sub>3</sub> ) <sub>2</sub> /THF	0.05	1200	55	400	S11
<b>S-rGO</b>	49	a non-nucleophilic electrolyte	0.01	448	50	236	S12
<b>S/NC</b>	76.2	0.4 mol L <sup>-1</sup> Mg[B(hfp) <sub>4</sub> ] <sub>2</sub> in DME	0.02	431	50	228	S13
<b>S@VN</b>	60	Mg(CF <sub>3</sub> SO <sub>3</sub> ) <sub>2</sub> -based electrolyte	0.3	575	100	450	S14
<b>S@MC</b>	55.8	0.25 mol L <sup>-1</sup> BMA + 2AlCl <sub>3</sub> +1.0 mol L <sup>-1</sup> LiCl /THF	0.04	700	100	400	S15
<b>MesoCo@C-S</b>	50	0.4 mol L <sup>-1</sup> MgCl <sub>2</sub> + AlCl <sub>3</sub> -DME	0.2	830	400	280	S16
<b>S@CNT</b>	80	0.5 mol L <sup>-1</sup> [Mg(DG) <sub>2</sub> ] [(HMDSAAlCl <sub>3</sub> ) <sub>2</sub> /DG	0.05	430	100	300	S17
<b>S/Ti<sub>3</sub>C<sub>2</sub>@CoO</b>	60	1 mol L <sup>-1</sup> Mg(TFSI) <sub>2</sub> / AlCl <sub>3</sub> / diglyme	0.06	1540	70	540	S18
<b>STAR@LCNC-S</b>	<b>71.3</b>	<b>MgCl<sub>2</sub>-LiCl/ THF (0.4 mol L<sup>-1</sup> MgCl<sub>2</sub>, 0.8 mol L<sup>-1</sup> LiCl)</b>	<b>0.5</b>	<b>1003</b>	<b>400</b>	<b>577.3</b>	<b>This work</b>

**Table S4.** The sulfur loading and areal capacity of different sulfur cathodes in the related reported reports after 50 cycles.

Cathode	S Loading (mg cm <sup>-2</sup> )	Areal capacity (mA h cm <sup>-2</sup> )	Cycling rate/C	Reference
KB/S	1	0.4	0.1	S3
S@ACC	1	0.4	0.1	S7
ZIF-C-S	1	0.6	0.1	S8
S@ACC	1	0.55	0.06	S9
S-rGO	1.5	0.35	0.01	S12
S/NC	3	0.68	0.02	S13
MesoCo@C-S	0.8	0.3	0.2	S16
S@CNT	0.65	0.17	0.05	S17
<b>STAR@LCNC-S</b>	<b>4</b>	<b>2.9</b>	<b>0.1</b>	<b>This work</b>

**Supplementary reference:**

- S1. Z. Zhang, Z. Cui, L. Qiao, J. Guan, H. Xu, X. Wang, P. Hu, H. Du, S. Li, X. Zhou, S. Dong, Z. Liu, G. Cui and L. Chen, *Adv. Energy Mater.*, 2017, **7**, 1602055.
- S2. R. K. Bhardwaj and A. J. Bhattacharyya, *ACS Appl. Energy Mater.*, 2021, **4**, 14121-14128.
- S3. Y. Ji, X. Liu-Théato, Y. Xiu, S. Indris, C. Njel, J. Maibach, H. Ehrenberg, M. Fichtner and Z. Zhao-Karger, *Adv. Funct. Mater.*, 2021, **31**, 2100868.
- S4. Q. Zhao, R. Wang, Y. Zhang, G. Huang, B. Jiang, C. Xu and F. Pan, *J. Magnesium Alloys*, 2021, **9**, 78-89.
- S5. D. Wu, W. Ren, Y. Yang, J. Wang and Y. NuLi, *J. Phys. Chem. C*, 2021, **125**, 25959-25967.
- S6. Z. Zhao-Karger, M. E. Gil Bardaji, O. Fuhr and M. Fichtner, *J. Mater. Chem. A*, 2017, **5**, 10815-10820.
- S7. Z. Zhao-Karger, R. Liu, W. Dai, Z. Li, T. Diemant, B. P. Vinayan, C. Bonatto Minella, X. Yu, A. Manthiram, R. J. Behm, M. Ruben and M. Fichtner, *ACS*

- Energy Lett.*, 2018, **3**, 2005-2013.
- S8. X. Zhou, J. Tian, J. Hu and C. Li, *Adv. Mater.*, 2018, **30**, 1704166.
- S9. T. Gao, S. Hou, F. Wang, Z. Ma, X. Li, K. Xu and C. Wang, *Angew. Chem. Int. Ed. Engl.*, 2017, **56**, 13526-13530.
- S10. Y. Yang, Y. Qiu, Y. NuLi, W. Wang, J. Yang and J. Wang, *J. Mater. Chem. A*, 2019, **7**, 18295-18303.
- S11. Y. Yang, W. Wang, Y. Nuli, J. Yang and J. Wang, *ACS Appl. Mater. Interfaces*, 2019, **11**, 9062-9072.
- S12. B. P. Vinayan, Z. Zhao-Karger, T. Diemant, V. S. Chakravadhanula, N. I. Schwarzburger, M. A. Cambaz, R. J. Behm, C. Kubel and M. Fichtner, *Nanoscale*, 2016, **8**, 3296-3306.
- S13. B. P. Vinayan, H. Euchner, Z. Zhao-Karger, M. A. Cambaz, Z. Li, T. Diemant, R. J. Behm, A. Gross and M. Fichtner, *J. Mater. Chem. A*, 2019, **7**, 25490-25502.
- S14. D. Huang, S. Tan, M. Li, D. Wang, C. Han, Q. An and L. Mai, *ACS Appl. Mater. Interfaces*, 2020, **12**, 17474-17480.
- S15. X. Zhao, Y. Yang, Y. NuLi, D. Li, Y. Wang and X. Xiang, *Chem. Commun.*, 2019, **55**, 6086-6089.
- S16. J. Sun, C. Deng, Y. Bi, K.-H. Wu, S. Zhu, Z. Xie, C. Li, R. Amal, J. Luo, T. Liu and D.-W. Wang, *ACS Appl. Energy Mater.*, 2020, **3**, 2516-2525.
- S17. Y. Xu, W. Li, G. Zhou, Z. Pan and Y. Zhang, *Energy Storage Mater.*, 2018, **14**, 253-257.
- S18. H. Xu, D. Zhu, W. Zhu, F. Sun, J. Zou, R. M. Laine and W. Ding, *Chem. Eng. J.*, 2022, **428**, 131031.
- S19. G. Kresse and J. Furthmüller, *Phys. Rev. B*, 1996, **54**, 11169-11186.
- S20. G. Kresse and D. Joubert, *Phys. Rev. B*, 1999, **59**, 1758.
- S21. J. P. Perdew, K. Burke and M. Ernzerhof, *Phys. Rev. Lett.*, 1996, **77**, 3865.
- S22. P. E. Blöchl, *Phys. Rev. B*, 1994, **50**, 17953.
- S23. V. Wang, N. Xu, J. C. Liu, G. Tang and W. T. Geng, *Comput. Phys. Commun.*,

2021, **267**, 108033.